ACS APPLIED MATERIALS & INTERFACES

Research Article

www.acsami.org

Autonomous Motion and Temperature-Controlled Drug Delivery of Mg/Pt-Poly(*N*-isopropylacrylamide) Janus Micromotors Driven by Simulated Body Fluid and Blood Plasma

Fangzhi Mou,[†,‡] Chuanrui Chen,[†,‡] Qiang Zhong,[†] Yixia Yin,[†] Huiru Ma,[§] and Jianguo Guan*[,†]

[†]State Key Laboratory of Advanced Technology for Materials Synthesis and Processing, Wuhan University of Technology, Wuhan 430070, People's Republic of China

[§]Department of Chemistry, Wuhan University of Technology, 122 Luoshi Road, Wuhan, 430070, People's Republic of China

Supporting Information

ABSTRACT: In this work, we have demonstrated the autonomous motion of biologically-friendly Mg/Pt-Poly(*N*-isopropylacrylamide) (PNIPAM) Janus micromotors in simulated body fluids (SBF) or blood plasma without any other additives. The pit corrosion of chloride anions and the buffering effect of SBF or blood plasma in removing the $Mg(OH)_2$ passivation layer play major roles for accelerating $Mg-H_2O$ reaction to produce hydrogen propulsion for the micromotors. Furthermore, the Mg/Pt-PNIPAM Janus micromotors can effectively uptake, transport, and temperature-control-release drug molecules by taking advantage of the partial surface-attached thermoresponsive PNIPAM hydrogel layers. The PNIPAM hydrogel layers on the micromotors can be easily replaced with other responsive polymers or antibodies by the surface modification strategy, suggesting that the as-proposed micromotors also hold a promising potential for separation and detection of heavy metal ions, toxicants, or proteins.

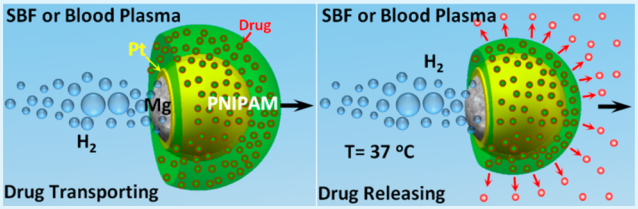

KEYWORDS: *micromotors, Janus particles, magnesium−water reaction, self-propulsion, autonomous motion, body fluid, blood plasma*

INTRODUCTION

Natural biomotors can autonomously move by taking advantage of the spontaneous hydrolysis of biological energy units, such as ATP.[1,2] Inspired by this, vastly growing efforts are currently being devoted to the design and fabrication of artificial micro/nanomotors that convert chemical energy into autonomous motion.[3−9] Until now, various self-propelled micro/nanomotors, such as the asymmetrical catalytic nanorods,[10,11] spherical Janus micromotors,[12−15] and tubular microengines,[16−19] have been developed based on the propulsion of bubbles, interfacial tension gradients, self-electrophoresis, or self-diffusiophoresis induced by asymmetrical chemical reactions. Due to their fascinating capabilities to pick up, transport, and release various micro/nanocargos in liquid media, they are expected to perform complex tasks in biological fluids ranging from targeted delivery of drugs,[20−23] to separation of proteins and cells,[24] to microsurgeries, etc.[25] However, most of the currently reported artificial micro/nanomotors are bioincompatible because of the critical requirement of using H_2O_2, acidic, alkaline, Br_2, or I_2 solutions as fuel sources, or the generation of toxic products such as Al and Ga ions.[4,26] In contrast, the recently developed Mg-based Janus micromotors, which were driven by the magnesium−water reaction in aqueous media with the assistance of concentrated inorganic salts (0.5 M $NaHCO_3$ or NaCl, etc.),[12,27] are biocompatible and may provide an opportunity to fabricate biocompatible micromotors with desired functionalities, which are best able to harvest energy directly from biological media (especially from blood or blood plasma) without any additives.

In this work, taking into account that blood plasma is a buffering aqueous liquid containing such anions as Cl^-, HCO_3^-, etc., and that poly(*N*-isopropylacrylamide) (PNIPAM) hydrogels show intriguing behaviors for uptake and temperature-controlled release of drugs,[28,29] we have developed a biocompatible Mg/Pt-PNIPAM Janus micromotor by a simple surface modification strategy, and for the first time demonstrated the autonomous motion, as well as the temperature-controlled drug delivery of synthetic micro/nanomotors in SBF and blood plasma without any introduced additives or fuels. The self-propulsion of the Janus micromotors is confirmed to be derived from Mg−water reaction under the promotion of Cl^- induced pit corrosion and the buffering effect from SBF and blood plasma. The Mg-based micromotors driven by SBF or blood plasma can be used as effective carriers for drugs, heavy metal ions, proteins, or cells with proper surface modifications.

Received: May 6, 2014
Accepted: May 28, 2014
Published: May 28, 2014

EXPERIMENTAL SECTION

In order to fabricate Mg/Pt-PNIPAM Janus micromotors, a simple asymmetric modification process (Scheme 1) similar to the previous

Scheme 1. Fabrication Process for the Mg/Pt-PNIPAM Janus Micromotors

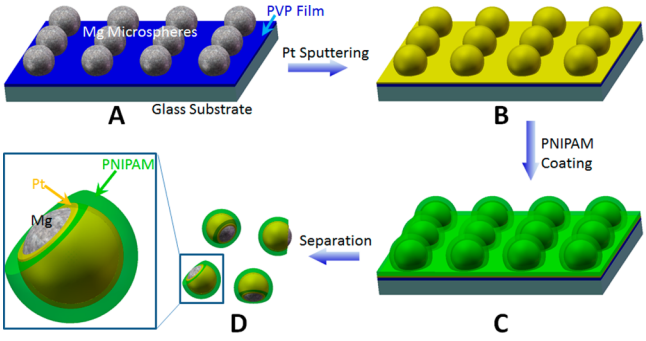

report for Mg microspheres was performed.[12] In detail, Mg microspheres (average sizes of 50 μm) were scattered on the surface of a glass slide precoated with a thin Polyvinylpyrrolidone (PVP) film (by dripping 100 μL 0.5 wt % PVP ethanol solution on the glass slide and drying it at 60 °C for 10 min). Then the glass slide was placed in humid air with a relative humidity of 80% for 5 s. During this process, the Mg spheres were partially immersed in the swollen PVP film by moisture absorption, and the bottom surfaces of Mg spheres were partially covered and fixed by PVP film. Then, the exposed Mg surfaces were coated with a platinum layer via ion sputtering for 240 s under a pressure of 0.6 Pa. To prepare poly(*N*-isopropylacrylamide) (PNIPAM) precursor solution, 0.35 g *N*-isopropylacrylamide (NIPAM) was dissolved in 3.5 mL ethylene glycol, followed by addition of 0.2 g bis(*N*,*N*-methylene bis(acrylamide)) and 20 μL DEAP (2,2-diethoxyacetophenone) into the solution. Then, 100 μL PNIPAM ethylene glycol precursor solution was dropped onto the glass slide to form a liquid film on the surface of the Mg/Pt microspheres fixed on the PVP-glass slide. Then the glass slide was exposed to the UV light to polymerize the NIPAM for 4 min. After being dried in vacuum at 60 °C for 12 h, the Mg/Pt-PNIPAM Janus micromotors were carefully separated from the substrate by a blade-scratching process, and washed with ethanol twice. The Mg-PNIPAM particles were prepared using a similar protocol, but without sputtering the Pt layer on the Mg surface. Scanning electron microscopy (SEM) and energy-dispersive X-ray (EDX) analyses were obtained by using a Hitachi S-4800 field-emission SEM (Japan).

Simulated body fluid (SBF)[28] and the solutions containing individual anions or components with the same concentrations as those in SBF were prepared according to Supporting Information (SI) Table S1. The pH value of the Cl^- solution was adjusted to 7.4 using 1 M HCl and NaOH solution, and the pH values of the HCO_3^-, HPO_4^{2-}, SO_4^{2-}, or Tris solutions were adjusted to 7.4 by adding 1 M H_2SO_4 and NaOH solution. The autonomous motion of the micromotor was observed and recorded at room temperature through an optical microscope (Olympus BX60), coupled with 4× and 10× objectives. All videos of the micromotor movement were analyzed using ImageJ and Origin 8.5 software (SI). Fluorescein isocyanate (FITC) was used as a model drug[21,30,31] to investigate the drug uptake, transportation, and release behaviors of the Mg/Pt-PNIPAM Janus micromotors. To load FITC into the micromotor, 3 mg Mg/Pt-PNIPAM Janus particles were dispersed in 4 mL FITC solution at 4 °C for 4 h in dark. After the drug loading process was accomplished, the suspension was centrifuged at 5000 rpm for 2 min to separate the FITC-loaded particles and washed with 2 mL cold water (4 °C) twice. The concentration of FITC in the solutions before and after the loading process, as well as in washed solutions were determined by using a fluorophotometer (Shimadzu PerkinElmer LS55) with an excitation wavelength of 488 nm and an emission wavelength of 520 nm. The drug loading efficiency is calculated as follows:

$$\text{loading efficiency} = \frac{\text{drug load } (\mu g)}{\text{dried weight (mg)}}$$

where "drug load" is the amount of drug loaded in the micromotors and "dried weight" is the dried weight of the micromotors.

To visualize the temperature-induced drug releasing process, a confocal laser scanning microscope (CLSM, leica DMIRE2) was used to observe the variation of the morphology and fluorescent intensity of the micromotor with the increasing temperature (from 20 to 37 °C) and releasing time (0−30 min) with an excitation wavelength of 488 nm and an emission wavelength of 520 nm. To avoid the influence of the releasing bubbles and the motion of the micromotor on the CLSM observation, the micromotor was soaked in pure water at 25 °C for 24 h before drug loading process, which could retard the reactivity of the micromotor with SBF. Typically, 100 μL of the aqueous suspension of Mg/Pt-PNIPAM Janus particles (0.2 g/L) were added to 3 mL SBF in a Perti dish. Then the Petri dish was heated from 20 to 37 °C and maintained at 37 °C for a period of 30 min using a microscope temperature control stage. The optical images were recorded every 30 s. To monitor the FITC releasing process from the micromotors at 20 and 37 °C versus time, the temperature of 3 mL SBF was maintained at 20 or 37 °C, respectively, for 10 min before 100 μL of the aqueous suspension (4 °C) of the micromotors (0.2 g/L) was added. Then, the fluorescent and optical images of the micromotors were recorded every 30 s using an $x-y-t$ model of the LCSM for 30 min, and the fluorescence intensity variation over the Mg/Pt-PNIPAM Janus micromotor was analyzed by the intensity measurement feature in the Leica confocal software version 2.61.

To evaluate the cytotoxicity of the Mg/Pt-PNIPAM Janus micromotors, hemolytic assay for the Mg/Pt-PNIPAM Janus micromotors and their fuel medium was conducted according to the reported procedure using the ethylenediamine tetra-acetic acid (EDTA)-stabilized human blood.[32] First, 5 mL of blood sample was added to 10 mL of PBS, and then red blood cells (RBCs) were isolated by centrifugation at 10 016*g* for 10 min. The RBCs were washed five times with 10 mL of PBS solution. The purified RBCs were diluted to a volume of 50 mL with PBS. RBCs' incubation with D.I. water and PBS were respectively used as the positive and negative controls. Then, 0.2 mL diluted RBC suspension was added to 0.8 mL SBF or PBS containing 0.05 g L^{-1} Mg/Pt-PNIPAM Janus micromotors, and allowed to stand for 3 h, and subsequently centrifuged at 10 016*g* for 3 min. 100 μL of the supernatant was transferred to a 96-well plate. The absorbance values of the supernatants at 570 nm were determined using a microplate reader with absorbance at 655 nm as a reference. The percent hemolysis of RBCs was calculated using the following formula:

$$\%\ \text{hemolysis} = -\frac{\text{sample abs.} - \text{neg. abs.}}{\text{pos. abs.} - \text{neg. abs.}} \times 100\%$$

where "sample abs." is the sample absorbance; "pos. abs." is the positive control absorbance; and "neg. abs." is the negative control absorbance.

RESULTS AND DISCUSSION

A two-step asymmetric modification process was adopted for the fabrication of Mg/Pt-PNIPAM Janus micromotors.[12] As illustrated in Scheme 1, Mg microspheres (SI Figure S1) were at first partially embedded in PVP film on a glass slide. Then, the top surface was subsequently coated with layers of platinum and PNIPAM via ion sputtering and UV polymerization processes, respectively. Over 90% of the Mg/Pt-PNIPAM Janus micromotors can finally be separated from the substrate by a blade-scratching process (SI Figure S2a). Figure 1A and its inset show the Mg/Pt-PNIPAM Janus microspheres partially embedded in the PVP film, whereas Figure 1B shows a typical Mg/Pt-PNIPAM Janus microsphere separated from the substrate. Both of them indicate that the particles have average

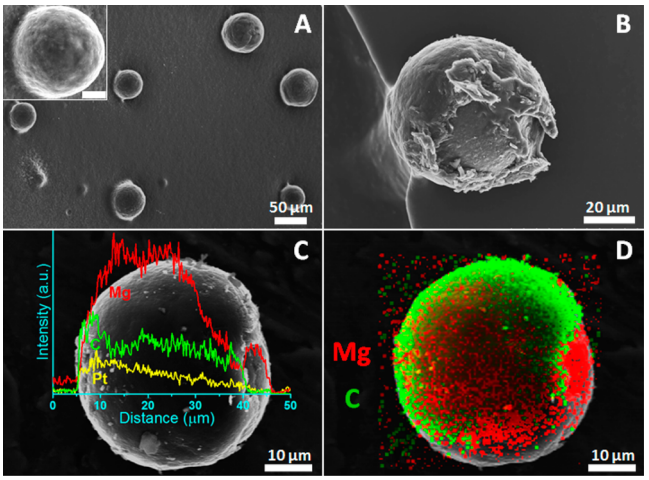

Figure 1. SEM images of Mg/Pt-PNIPAM Janus particles partially embedded in the substrate (A) and a separated Janus particle (B); elemental linear (C) and mapping (D) EDX analysis for a typical Janus particle; Scale bar in the inset of A is 10 μm.

diameters of about 50 μm. A binary heterostructure is obviously discernible from Figure 1B, in which about 3/4 of the surface of the Mg microsphere is covered by an asymmetric spherical-cap Pt-PNIPAM layer with a thickness of about 4 μm. The elemental linear (Figure 1C) and mapping (Figure 1D) EDX analyses indicate that the Mg signal is detected over the whole particle, whereas Pt and C signals can only be detected in the asymmetric spherical-cap, further confirming that the Mg/Pt-PNIPAM Janus particles are obtained, in which Mg microspheres are subsequently covered by asymmetric spherical-cap layers of Pt and PNIPAM.

To mimic the autonomous movement of the Mg/Pt-PNIPAM Janus micromotor in human blood plasma environments, simulated body fluid (SBF) containing 5 wt % PVP was selected as a carrier fluid. Here, the addition of PVP into SBF was mainly to make the viscosity of SBF close to that of blood plasma.[33] SI Video S1 and Figure 2 illustrate the self-propulsion of an Mg/Pt-PNIPAM Janus micromotor in SBF containing 5 wt % PVP. The typical time-lapse images (Figure 2A–D) taken from SI Video S1 shows that a long tail of hydrogen bubbles with diameters (R) of ca. 10 μm was generated on one side of the micromotor with a frequency (f) of about 90 Hz. This

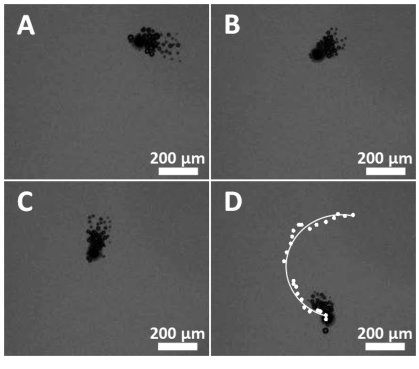

Figure 2. Time-lapse images of a typical Mg/Pt-PNIPAM Janus micromotor suspended in SBF with 5 wt % PVP taken from SI Video S1, illustrating the motor propulsion at a time interval of (A) 0, (B) 2, (C) 4, and (D) 8 s; the white dots and curve in D indicate the motion trajectory of the typical Mg/Pt-PNIPAM Janus micromotor.

reflects the spontaneous and rapid reaction of Mg with water in SBF, as illustrated in eq 1.[34]

$$Mg(s) + 2H_2O(aq) = Mg(OH)_2(s) + H_2(g) + \Delta_r{}^{\theta}G \quad (1)$$

The as-generated bubbles engender a strong momentum that propels the micromotor forward with a speed of 95 μm s^{-1}, representing the conversion of chemical energy into autonomous motion. The speed is comparable to that of the spherical Janus micromotors driven by chemical corrosion of active metal.[12,15,27] The power conversion efficiency (η_c) of the micromotor, defined as the ratio of the output mechanical power (P_{mecha}) into the input overall chemical power (P_{chem}),[35] can be estimated from eq 2 to be 1.9×10^{-19}.

$$\eta_c = \frac{P_{mecha}}{P_{chem}} = \frac{F_{drag}v}{n_{H_2}\Delta_r G^{\theta}} = \frac{6\pi\mu r v^2}{n_{H_2}\Delta_r G^{\theta}} \quad (2)$$

Here, F_{drag} is the drag force on the spherical micromotor, v is the speed of the micromotor (95 μm s^{-1}), μ is the dynamic viscosity of SBF containing 5 wt % PVP (2.2 mPa · s), r is the radius of the micromotor (ca. 50 μm), $n_{H_2} = ((4/3)(\pi R^3 f)/(22.4 \times 10^{-3}))$ is the hydrogen evolution rate from the micromotor in units of mol·(motor·s)$^{-1}$, and $\Delta_r G^{\theta}$ is the Gibbs free energy of Mg–water reaction (eq 1, −596.4 kJ per mole of H_2 produced). As the curve shown in Figure 2D, the Mg/Pt-PNIPAM Janus micromotor in SBF moves following a curved ballistic trajectory due to the deviation of the H_2 releasing direction from the symmetry axis of the Janus micromotor, generating a rotational torque besides the translational propulsion. The typical life span (SI Figure S3) and moving distance of the motor are about 60 s and several millimeters, respectively. Both of them are similar to those of active metal-based micromotors.[12,19,26] This implies that the coating layer of PNIPAM has little influence on the motion of the micromotor. Further prolonging the lifetime of the Mg-based micromotors is currently underway by optimizing the size and number of exhaust nozzles.

Rapidly removing the $Mg(OH)_2$ passivation layer on the exposed Mg surface to promote Mg–H_2O reaction is crucial for the as-developed Mg/Pt-PNIPAM Janus micromotor to attain autonomous motion.[12] SBF is a buffering solution containing certain concentrations of HCO_3^-, Cl^-, HPO_4^{2-}, and SO_4^{2-} anions. In order to investigate the effect of anions in SBF or blood plasma on the self-propulsion of the Mg/Pt-PNIPAM Janus micromotors, the micromotors are added into aqueous solutions with HCO_3^-, Cl^-, HPO_4^{2-}, or SO_4^{2-} of the same concentration as that in SBF, respectively. Figure 3 and SI Video S2 show that no bubble generation is observed on the micromotors in the solutions containing 2.5 mM SO_4^{2-}, 1 mM HPO_4^{2-}, or 27 mM HCO_3^-. In contrast, there are numerous bubbles generated swiftly in both the solution containing 125 mM Cl^- and that containing 50 mM Tris. This confirms that low concentrated sulfate solution has a weak effect on the removal of the $Mg(OH)_2$ passivation layer. Hydrogen phosphate cannot make the Mg–water reaction incessantly occur as the $Mg_3(PO_4)_2$ produced by consuming OH^- has a lower solubility product constant (K_{sp}) (= 1.04×10^{-24}) than that for $Mg(OH)_2$ (= 5.6×10^{-12}), and will also tightly attach on the Mg surface.[34] HCO_3^- may accelerate the Mg–water reaction at a concentration above 100 mM due to the greater K_{sp} for $MgCO_3$ (= 6.8×10^{-6}) than that for $Mg(OH)_2$,[12] but its concentration in SBF is too low (27 mM) to peel off the

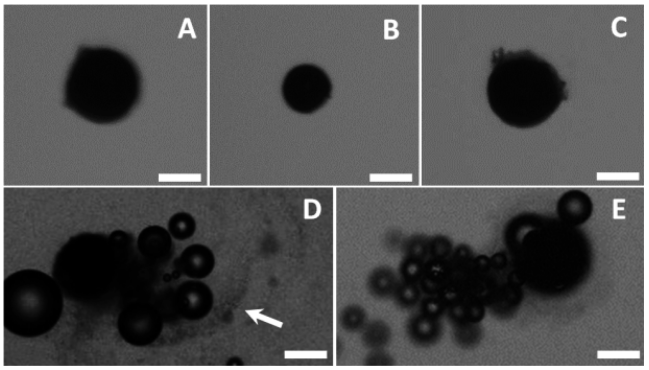

Figure 3. Images of the Mg/Pt-PNIPAM micromotor in aqueous solutions containing only (A) 2.5 mM SO_4^{2-}, (B) 1 mM HPO_4^{2-}, (C) 27 mM HCO_3^-, (D) 125 mM Cl^-, or (E) 50 mM Tris-HCl buffered solution, taken from SI Video S2. Scale bar, 50 μm.

$Mg(OH)_2$ passivation layer. The chloride-induced pitting corrosion on the Mg surface, especially with the additional galvanic corrosion between Mg and Pt (corresponding to anodic indexes of −1.75 and −0.0 V, respectively) can remarkably engender bubble propulsion of the micromotor, which is consistent with the results reported by Wang's group.[27] However, with the H_2 bubbles released (about 60 Hz in *f*), there exist solid precipitates discharged from the micromotor in the solution containing only Cl^- ions, as indexed in Figure 3D by a white arrow. This phenomenon is not observed when the micromotor moves in SBF, suggesting that the Tris-HCl buffer in SBF plays an important role in the dissolution of $Mg(OH)_2$ precipitates because other anions (2.5 mM SO_4^{2-}, 1 mM HPO_4^{2-}, or 27 mM HCO_3^-) have a negligible effect on the dissolution of $Mg(OH)_2$ (Figure 3A–C). This implies that the Tris-HCl buffer solution can provide protons to consume the OH^- anions generated from Mg–H_2O reaction and inhibit the formation of an $Mg(OH)_2$ passive layer or $Mg(OH)_2$ precipitates.[34,36] As a result, it facilitates the Mg–H_2O reaction and contributes to the propulsion of the micromotor (Figure 3E). In a word, besides the galvanic corrosion and Cl^- induced pit corrosion,[27] the strong buffering effect of the SBF plays a dominant role in the self-propulsion of the Mg/Pt-PNIPAM micromotor in SBF. In addition, it is also possible for the HCO_3^- and HPO_4^{2-} anions in SBF to make some additional contributions as buffering agents.

In the as-fabricated Mg/Pt-PNIPAM Janus micromotor, the asymmetric middle nanolayer of Pt is indispensable for the asymmetrical generation of hydrogen bubbles and the efficient self-propulsion. SI Figure S4A and SI Video S3 show that Mg/PNIPAM Janus microsphere, which is fabricated according to Scheme 1 but without the step of Pt sputtering, exhibits a motion in SBF as slow as about 15 μm s^{-1}. In contrast, the Mg/Pt Janus microsphere is self-propelled by asymmetrically released H_2 bubbles at a high speed of over 105 μm s^{-1} in SBF (SI Figure S4B and SI Video S3). This suggests that the asymmetric spherical-cap layer of PNIPAM cannot be substituted for that of Pt to effectively suppress Mg–H_2O reaction at the covered Mg surface, since it forms a three-dimensional hydrogel in SBF at room temperature so that H_2O molecules, etching anions of HCO_3^- and Cl^- in SBF, as well as generated hydrogen bubbles all can penetrate this hydrogel layer.

As depicted in Scheme 2, the Mg/Pt-PNIPAM Janus micromotors exhibit excellent drug uptake, transportation,

Scheme 2. Demonstration of the Drug (A, B) Loading, (C) Transporting, and (D) Releasing Behaviors of the Mg/Pt-PNIPAM Janus Micromotors

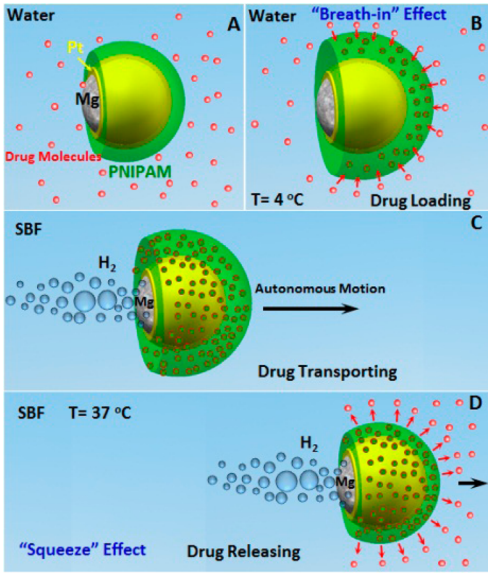

and temperature-controlled release behaviors, thanks to the partial surface-attached thermoresponsive PNIPAM shell. For example, they can load fluorescein isocyanate (FITC), used as a model drug here,[21,30,31] by the temperature-induced "breath-in" effect of the PNIPAM hydrogel shells,[29] after soaking them in FITC solution at 4 °C for 4 h. The drug loading efficiency (DLE) of the micromotors reaches 8.1 μg/mg in our experiment. When the FITC-loaded micromotor is put into SBF, it autonomously moves (SI Video S4). This clearly illustrates the capability to transport drug molecules, as shown in Scheme 2C and Figure 4.

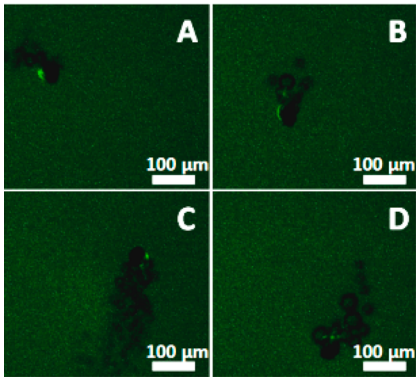

Figure 4. Time-lapse fluorescent images of the autonomous motion of the Mg/Pt-PNIPAM micromotor loaded with FITC in SBF containing 5 wt % PVP (SI Video S4) at an interval of (A) 0, (B) 2, (C) 4, and (D) 7 s.

SI Video S5 (with 300× speed acceleration) and Figure 5A present the fluorescent intensity variation over two typical Mg/Pt-PNIPAM Janus micromotor at 20 and 37 °C versus time. It can be seen that the fluorescent intensity of the PNIPAM hydrogel layer on the micromotor decreases sharply with a prolongation of the soaking time. This, compared with the negligible fluorescent intensity decrease of the FITC in SBF (SI Figure S5), represents the releasing process of the FITC

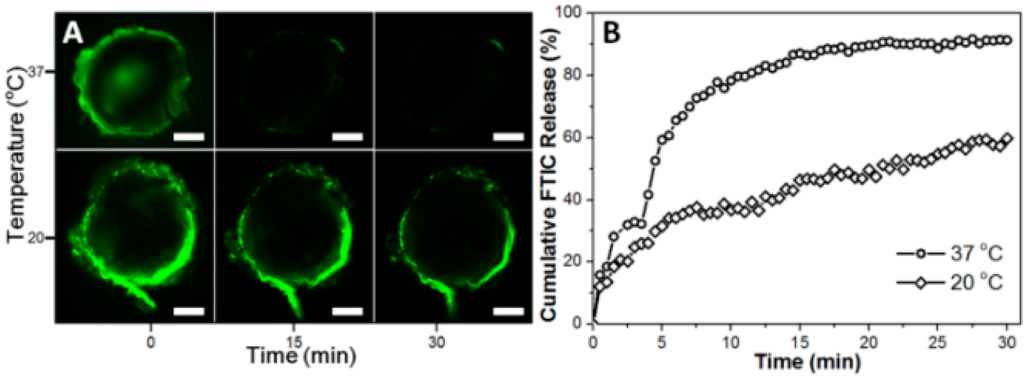

Figure 5. (A) Fluorescent images representing the drug release from the Mg/Pt-PNIPAM Janus micromotor and (B) the normalized average cumulative drug release profiles at 20 and 37 °C versus time; Scale bars in A: 10 μm.

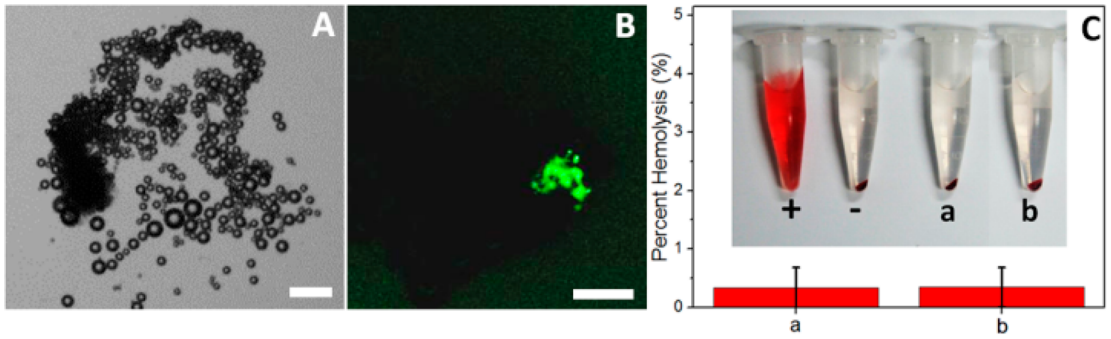

Figure 6. (A) Optical and (B) fluorocent images of the self-propulsion of the FITC-loaded Mg/Pt-PNIPAM micromotor in human blood plasma; scale bars: 100 μm. (C) Hemolytic assay for the 0.05 g L^{-1} Mg/Pt-PNIPAM Janus micromotors in (a) PBS and (b) SBF. Evaluation scale: highly hemocompatible (less than 5% hemolysis); hemocompatible (5−10% hemolysis); nonhemocompatible (over 20% hemolysis). The inset shows the corresponding hemolysis photographs of RBCs. The presence of red hemoglobin in the supernatant indicates damaged RBCs. PBS (−) and D.I. water (+) are used as negative and positive controls, respectively.

molecules. Figure 5B further indicates quantitatively that for the Mg/Pt-PNIPAM Janus micromotor, the release rate of FITC at 37 °C becomes much faster than that at 20 °C, and almost reaches its equilibrium at about 15 min, revealing that the drug-releasing behavior from the micromotor can be controlled by the environmental temperature (T). This is because the PNIPAM hydrogel layer of the micromotor in SBF possesses a volume phase transition temperature (VPTT) at 30 °C.[37] At T = 20 °C, the drugs release mainly in a molecular diffusion processes or osmosis transport mechanism because of the FTIC concentration gradient between the surrounding water media and the PNIPAM hydrogel layers. The faster release rate at T = 37 °C is ascribed to a combination of the increasing system's kinetic energy and the "squeezing" mechanism due to the shrinkage of the PNIPAM hydrogel layers with the increase of T, as verified by the results in SI Figure S6.[30] In addition, in the FITC releasing curve at the period of 3−5 min at 37 °C, a plateau exists between two sharp releases of FITC. This could be explained by the "skin-effect" of PNIPAM when T is higher than its VPTT.[30,38] In detail, when the Mg/Pt-PNIPAM micromotor loaded with FITC at 4 °C is added to an SBF at 37 °C, a temperature gradient across the PNIPAM gel will form and make a burst release of the surface FITC (0−3 min in Figure 5B), accompanying the formation of a dense "skin" on the surface of the PNIPAM gel. Afterward, the release of FITC was greatly hindered due to this "skin-effect" (3−5 min in Figure 5B). When the temperature of the inner PNIPAM gel increases above VPTT with increasing soaking time, the hydrostatic pressure inside the gel will finally build up and cause the collapses of polymer networks, "squeezing" out the fluid containing FITC (the burst release after 5 min in Figure 5B). The above results suggest that the proposed Mg/Pt-PNIPAM Janus micromotor is capable of loading, transporting, and controlled-releasing drugs in SBF, as illustrated in Scheme 2. It is imaginable that the drug releasing critical temperature of the micromotors can be simply modulated by adjusting the copolymerization of NIPAM with comonomers.

As the chemical composition and properties of SBF are similar to those of human blood plasma, except serum albumin and proteins etc., the as-proposed Mg/Pt-PNIPAM Janus micromotors are expected to show self-propulsion, as well as controlled drug delivery in blood plasma. SI Video S6 and Figure 6A show that the Mg/Pt-PNIPAM Janus micromotor autonomously move in human blood plasma with a speed of about 35 μm s^{-1}. In contrast, the Pt-based catalytic tubular micromotor is unable to move in the human blood plasma (even with 3 wt % H_2O_2 addition) because of the coverage of active sites by the contained proteins and its high viscosity.[39] It is also noted that the speed is slower than that in SBF. This is mainly because albumin can keep the generated bubbles stabilized and attached to the micromotor,[40] burdening the movement of the micromotor. Figure 6A further indicates that the ejected H_2 bubbles have a diameter of about 10 μm (similar to that of RBCs), implying that they may display similar rheology in microvessels and capillaries to RBCs, and have no adverse effects to the human body for their potential in vivo applications.[40] The florescent image (Figure 6B) and video in SI Video S6 shows the autonomous motion of the FITC-loaded

Mg/Pt-PNIPAM micromotor in human blood plasma, suggesting the promising capability to transport and release drugs in human blood plasma. In addition, Figure 6C shows that the percentages of hemolysis are all within 1% for the Mg/Pt-PNIPAM micromotor with or without SBF, suggesting that the Janus micromotor and their autonomous motion have a negligible influence on the damage of red blood cells (RBCs, highly hemocompatible) and are friendly to organisms.

CONCLUSIONS

We have demonstrated the autonomous motion of the biologically-friendly Mg/Pt-PNIPAM Janus micromotors in SBF or blood plasma without any other additives. The pit corrosion of chloride anions and the buffering effect of SBF or blood plasma in removing the $Mg(OH)_2$ passivation layer play major roles for accelerating $Mg-H_2O$ reaction to produce hydrogen propulsion for the micromotors. Furthermore, the Mg/Pt-PNIPAM Janus micromotors can effectively uptake, transport, and temperature-control-release drug molecules by taking advantage of the partial surface-attached thermoresponsive PNIPAM hydrogel layers. The PNIPAM hydrogel layers on the micromotors can be easily replaced with other responsive polymers or antibodies by the surface modification strategy, suggesting that the as-proposed micromotors also hold a promising potential for in vitro separation and detection of heavy metal ions, toxicants, or proteins. Future efforts should be devoted to improving the motility control, power conversion efficiency, and lifetime of the Mg-based motors to meet the requirements of their potential in vivo applications, such as by elaborately designing the nozzle exits.

ASSOCIATED CONTENT

Supporting Information

SEM images of Mg microspheres and microscopic observation of self-propulsion and morphology of the micromotors (Videos S1–S6). This material is available free of charge via the Internet at http://pubs.acs.org.

AUTHOR INFORMATION

Corresponding Author

*Tel: 86-27-87218832; fax: 86-27-87879468; e-mail: guanjg@whut.edu.cn.

Author Contributions

‡These authors contributed equally to this work.

Funding

National Natural Science Foundation of China (51303144), the Top Talents Lead Cultivation Project and Natural Science Foundation of Hubei Province (2012FFB05101), the Self-determined and Innovative Research Funds of SKLWUT and Wuhan University of Technology (2013-PY-3), the Fundamental Research Funds for the Central Universities (WUT: 2013-IV-089).

Notes

The authors declare no competing financial interest.

ACKNOWLEDGMENTS

This work was supported by the National Natural Science Foundation of China (51303144), the Top Talents Lead Cultivation Project and Natural Science Foundation of Hubei Province (2012FFB05101), the Self-Determined and Innovative Research Funds of SKLWUT and Wuhan University of Technology (2013-PY-3), and the Fundamental Research Funds for the Central Universities (WUT: 2013-IV-089).

REFERENCES

(1) Schliwa, M.; Woehlke, G. Molecular Motors. *Nature* **2003**, *422*, 759–765.
(2) Spudich, J. A. Molecular Motors, Beauty in Complexity. *Science* **2011**, *331*, 1143–1144.
(3) Gao, W.; Wang, J. The Environmental Impact of Micro/Nanomachines: A Review. *ACS Nano* **2014**, *8*, 3170–3180.
(4) Wang, W.; Duan, W.; Ahmed, S.; Mallouk, T. E.; Sen, A. Small Power: Autonomous Nano- and Micromotors Propelled by Self-Generated Gradients. *Nano Today* **2013**, *8*, 531–554.
(5) Sengupta, S.; Ibele, M. E.; Sen, A. Fantastic Voyage: Designing Self-Powered Nanorobots. *Angew. Chem., Int. Ed.* **2012**, *51*, 8434–8445.
(6) Ozin, G. A.; Manners, I.; Fournier-Bidoz, S.; Arsenault, A. Dream Nanomachines. *Adv. Mater.* **2005**, *17*, 3011–3018.
(7) Wilson, D. A.; Nolte, R. J. M.; van Hest, J. C. M. Autonomous Movement of Platinum-Loaded Stomatocytes. *Nat. Chem.* **2012**, *4*, 268–274.
(8) Wang, J.; Gao, W. Nano/Microscale Motors: Biomedical Opportunities and Challenges. *ACS Nano* **2012**, *6*, 5745–5751.
(9) Sundararajan, S.; Lammert, P. E.; Zudans, A. W.; Crespi, V. H.; Sen, A. Catalytic Motors for Transport of Colloidal Cargo. *Nano Lett.* **2008**, *8*, 1271–1276.
(10) Paxton, W. F.; Kistler, K. C.; Olmeda, C. C.; Sen, A.; St. Angelo, S. K.; Cao, Y.; Mallouk, T. E.; Lammert, P. E.; Crespi, V. H. Catalytic Nanomotors: Autonomous Movement of Striped Nanorods. *J. Am. Chem. Soc.* **2004**, *126*, 13424–13431.
(11) Liu, R.; Sen, A. Autonomous Nanomotor Based on Copper–Platinum Segmented Nanobattery. *J. Am. Chem. Soc.* **2011**, *133*, 20064–20067.
(12) Mou, F.; Chen, C.; Ma, H.; Yin, Y.; Wu, Q.; Guan, J. Self-Propelled Micromotors Driven by the Magnesium–Water Reaction and Their Hemolytic Properties. *Angew. Chem., Int. Ed.* **2013**, *52*, 7208–7212.
(13) Howse, J. R.; Jones, R. A. L.; Ryan, A. J.; Gough, T.; Vafabakhsh, R.; Golestanian, R. Self-Motile Colloidal Particles: From Directed Propulsion to Random Walk. *Phys. Rev. Lett.* **2007**, *99*, 048102.
(14) Baraban, L.; Makarov, D.; Streubel, R.; Moench, I.; Grimm, D.; Sanchez, S.; Schmidt, O. G. Catalytic Janus Motors on Microfluidic Chip: Deterministic Motion for Targeted Cargo Delivery. *ACS Nano* **2012**, *6*, 3383–3389.
(15) Gao, W.; D'Agostino, M.; Garcia-Gradilla, V.; Orozco, J.; Wang, J. Multi-Fuel Driven Janus Micromotors. *Small* **2013**, *9*, 467–471.
(16) Mei, Y.; Huang, G.; Solovev, A. A.; Ureña, E. B.; Mönch, I.; Ding, F.; Reindl, T.; Fu, R. K. Y.; Chu, P. K.; Schmidt, O. G. Versatile Approach for Integrative and Functionalized Tubes by Strain Engineering of Nanomembranes on Polymers. *Adv. Mater.* **2008**, *20*, 4085–4090.
(17) Manesh, K. M.; Cardona, M.; Yuan, R.; Clark, M.; Kagan, D.; Balasubramanian, S.; Wang, J. Template-Assisted Fabrication of Salt-Independent Catalytic Tubular Microengines. *ACS Nano* **2010**, *4*, 1799–1804.
(18) Solovev, A. A.; Mei, Y. F.; Urena, E. B.; Huang, G. S.; Schmidt, O. G. Catalytic Microtubular Jet Engines Self-Propelled by Accumulated Gas Bubbles. *Small* **2009**, *5*, 1688–1692.
(19) Gao, W.; Uygun, A.; Wang, J. Hydrogen-Bubble-Propelled Zinc-Based Microrockets in Strongly Acidic Media. *J. Am. Chem. Soc.* **2012**, *134*, 897–900.
(20) Wu, Z. G.; Wu, Y. J.; He, W. P.; Lin, X. K.; Sun, J. M.; He, Q. Self-Propelled Polymer-Based Multilayer Nanorockets for Transportation and Drug Release. *Angew. Chem., Int. Ed.* **2013**, *52*, 7000–7003.
(21) Wu, Y.; Wu, Z.; Lin, X.; He, Q.; Li, J. Autonomous Movement of Controllable Assembled Janus Capsule Motors. *ACS Nano* **2012**, *6*, 10910–10916.

(22) Kagan, D.; Laocharoensuk, R.; Zimmerman, M.; Clawson, C.; Balasubramanian, S.; Kang, D.; Bishop, D.; Sattayasamitsathit, S.; Zhang, L.; Wang, J. Rapid Delivery of Drug Carriers Propelled and Navigated by Catalytic Nanoshuttles. *Small* **2010**, *6*, 2741−2747.
(23) Gao, W.; Kagan, D.; Pak, O. S.; Clawson, C.; Campuzano, S.; Chuluun-Erdene, E.; Shipton, E.; Fullerton, E. E.; Zhang, L.; Lauga, E.; Wang, J. Cargo-Towing Fuel-Free Magnetic Nanoswimmers for Targeted Drug Delivery. *Small* **2012**, *8*, 460−467.
(24) Balasubramanian, S.; Kagan, D.; Hu, C. M. J.; Campuzano, S.; Lobo-Castanon, M. J.; Lim, N.; Kang, D. Y.; Zimmerman, M.; Zhang, L. F.; Wang, J. Micromachine-Enabled Capture and Isolation of Cancer Cells in Complex Media. *Angew. Chem., Int. Ed.* **2011**, *50*, 4161−4164.
(25) Solovev, A. A.; Xi, W.; Gracias, D. H.; Harazim, S. M.; Deneke, C.; Sanchez, S.; Schmidt, O. G. Self-Propelled Nanotools. *ACS Nano* **2012**, *6*, 1751−1756.
(26) Gao, W.; Pei, A.; Wang, J. Water-Driven Micromotors. *ACS Nano* **2012**, *6*, 8432−8438.
(27) Gao, W.; Feng, X.; Pei, A.; Gu, Y.; Li, J.; Wang, J. Seawater-Driven Magnesium Based Janus Micromotors for Environmental Remediation. *Nanoscale* **2013**, *5*, 4696−4700.
(28) Cüneyt Tas, A. Synthesis of Biomimetic Ca−Hydroxyapatite Powders at 37°C in Synthetic Body Fluids. *Biomaterials* **2000**, *21*, 1429−1438.
(29) Guan, Y.; Zhang, Y. PNIPAM Microgels for Biomedical Applications: from Fispersed Particles to 3D Assemblies. *Soft Matter* **2011**, *7*, 6375−6384.
(30) Trongsatitkul, T.; Budhlall, B. M. Microgels or Microcapsules? Role of Morphology on the Release Kinetics of Thermoresponsive PNIPAm-*co*-PEGMa Hydrogels. *Polym. Chem.* **2013**, *4*, 1502−1516.
(31) Tong, G.-X.; Liu, F.-T.; Wu, W.-H.; Tong, C.-L.; Qiao, R.; Guo, H.-C. Facile Bubble-Assisted Evaporation-Induced Assembly of High-Density Arrays of Co_3O_4 Nano/Microlotus Leaves: Fluorescent Properties, Drug delivery, and Biocompatibility. *CrystEngComm* **2014**, *16*, 1645−1651.
(32) Lin, Y.-S.; Haynes, C. L. Impacts of Mesoporous Silica Nanoparticle Size, Pore Ordering, and Pore Integrity on Hemolytic Activity. *J. Am. Chem. Soc.* **2010**, *132*, 4834−4842.
(33) Rosenson, R. S.; McCormick, A.; Uretz, E. F. Distribution of Blood Viscosity Values and Biochemical Correlates in Healthy Adults. *Clin. Chem.* **1996**, *42*, 1189−1195.
(34) Jang, Y.; Collins, B.; Sankar, J.; Yun, Y. Effect of Biologically Relevant Ions on the Corrosion Products Formed on Alloy AZ31B: An Improved Understanding of Magnesium Corrosion. *Acta Biomater.* **2013**, *9*, 8761−8770.
(35) Wang, W.; Chiang, T.-Y.; Velegol, D.; Mallouk, T. E. Understanding the Efficiency of Autonomous Nano- and Microscale Motors. *J. Am. Chem. Soc.* **2013**, *135*, 10557−10565.
(36) Guard, L. M.; Hazari, N. Synthesis and Reactivity of Magnesium Complexes Supported by Tris(2-dimethylaminoethyl)amine (Me6t-ren). *Organometallics* **2013**, *32*, 2787−2794.
(37) Zhang, Y.; Furyk, S.; Bergbreiter, D. E.; Cremer, P. S. Specific Ion Effects on the Water Solubility of Macromolecules: PNIPAM and the Hofmeister Series. *J. Am. Chem. Soc.* **2005**, *127*, 14505−14510.
(38) Hoffman, A. S. Applications of Thermally Reversible Polymers and Hydrogels in Therapeutics and Diagnostics. *J. Controlled Release* **1987**, *6*, 297−305.
(39) Zhao, G.; Viehrig, M.; Pumera, M. Challenges of The Movement of Catalytic Micromotors in Blood. *Lab Chip* **2013**, *13*, 1930−1936.
(40) Sirsi, S. R.; Borden, M. A. Microbubble Compositions, Properties and Biomedical Applications. *Bubble Sci. Eng. Technol.* **2009**, *1*, 3−17.